Road Materials and Pavement Design

ISSN: (Print) (Online) Journal homepage: https://www.tandfonline.com/loi/trmp20

Mechanism-based evaluation of compactability of asphalt mixtures

Tianhao Yan, Mihai O. Marasteanu & Jia-Liang Le

To cite this article: Tianhao Yan, Mihai O. Marasteanu & Jia-Liang Le (2021) Mechanism-based evaluation of compactability of asphalt mixtures, Road Materials and Pavement Design, 22:sup1, S482-S497, DOI: 10.1080/14680629.2021.1905697

To link to this article: https://doi.org/10.1080/14680629.2021.1905697

Published online: 13 Apr 2021.

ROAD MATERIALS AND PAVEMENT DESIGN
2021, VOL. 22, NO. S1, S482–S497
https://doi.org/10.1080/14680629.2021.1905697

Mechanism-based evaluation of compactability of asphalt mixtures

Tianhao Yan , Mihai O. Marasteanu and Jia-Liang Le

Department of Civil, Environmental, and Geo- Engineering, University of Minnesota, Minneapolis, MN, USA

ABSTRACT

Compaction of asphalt mixtures is a critical component of the construction process of asphalt pavements. The quality of compaction has a significant consequence for the durability of asphalt pavements. Compaction of asphalt mixtures is a complex physical process, which has not been fully understood. In this study, we investigate the physical mechanisms of compaction, based on which we propose a new method to evaluate the compactability of asphalt mixtures. Two mesoscopic physical mechanisms are introduced. One is related to the jamming of aggregates, which governs the densification process of the mixture. The other is related to the binder-aggregate interaction, which is responsible for the change of shear resistance of mixtures during compaction. Based on these mechanisms, different indices are proposed to characterise the compactability of asphalt mixtures. The model is applied to analyse seven asphalt mixtures that were used to construct test sections at MnROAD research facility. Statistical analysis is performed to identify correlations between the compactability indices and material compositions, such as gradation and binder content. Based on the most significant correlations, multiple linear regression models are developed, which can be used to design more compactable mixtures.

ARTICLE HISTORY
Received 10 June 2020
Accepted 14 March 2021

KEYWORDS
Compaction; asphalt mixture; physical mechanisms; aggregates jamming; binder-aggregate interaction; mixture design

1. Introduction

During the construction of asphalt pavements, asphalt mixture is compacted from a loose state to a dense state by a combination of compression, shear and vibration forces. In this process, air voids are extruded out from the mixture and the internal aggregate structure is rearranged to a state such that some level of aggregate interlocking is achieved. Numerous studies have emphasised the paramount importance of compaction in building a durable and resilient pavement (Finn & Epps, 1980; Hughes, 1989; Linden et al., 1989; Vivar & Haddock, 2006).

Despite the significant research efforts devoted to understanding the compaction process, inadequate compaction is still a common problem in current practice. A previous study investigated 40 construction projects in the United States, and it showed that 55% of them had as-constructed densities less than 92% of the theoretical maximum specific gravity, G_{mm}, and 78% projects had as-constructed densities less than desired value of 93% of G_{mm} (Prowell & Brown, 2007). The average ultimate density was 94.6% of G_{mm}, which is considerably lower than the design value (96% of G_{mm}). Inadequate compaction has a significant adverse impact on durability, causing pavement distresses such as cracking, moisture damage and ravelling to initiate at early ages of pavement service life (Brown et al., 2004; Harmelink & Aschenbrener, 2002; Prowell & Brown, 2007).

CONTACT Tianhao Yan yan00004@umn.edu

The primary reason for inadequate field compaction is the low compactability of asphalt mixtures. In the United States, the current Superpave mix design method (AASHTO R35, 2017) was developed in the 1990s to mainly control rutting, which was the most prevalent distress at that time. To prevent rutting, the design emphasised stiffer mixture after construction, while the effect on compactability during construction was mainly disregarded. After the implementation of Superpave, durability related distresses, such as cracking and ravelling, became the most prevalent (West et al., 2018).

To ensure good durability of asphalt pavement, the compactability of mixtures must be considered in the design phase. Moutier (1974) studied the laboratory gyratory compaction of asphalt mixture and observed an approximate linear correlation between density and logarithm of number of gyrations. Subsequent studies have focused on the energy dissipation during the compaction process of asphalt mixtures (Dessouky et al., 2004; Faheem & Bahia, 2004; Guler et al., 2000; Stakston & Bahia, 2003). Based on the idea of energy dissipation, different energy indices were proposed to evaluate the compactability of mixtures (Dessouky et al., 2004; Faheem & Bahia, 2004; Stakston & Bahia, 2003). Though slightly different from each other, all of the energy indices were defined as the integration of a certain region of the compaction curve. Though the slope of linear correlation and the energy indices serve as global indictors of the overall compactability of mixtures, they are phenomenological in nature. There is a lack of understanding how these indicators are related to the physical mechanisms of the compaction process.

To explore the physical mechanism of the compaction process, the concept of locking point was proposed (Vavrik & Carpenter, 1998). The locking point is defined as the number of gyration at which aggregates interlock with each other, and further compaction of mixture becomes very hard. While slightly different definitions of locking point have been proposed (Pine, 1997; Shamsi & Mohammad, 2010; Vavrik & Carpenter, 1998), they all share the same physical interpretation, which is that compaction process essentially stops after aggregates interlocking is achieved. However, locking of aggregates cannot explain how the shear force generated from the gyratory motion affects the compaction. Without shear, the static pressure alone can only compact mixture to a very limited level.

The gyratory compaction is a complex process. At the compaction temperature, the mixture is multiphase, involving solid aggregates, liquid asphalt binder, and air. Also, different phases are coupled; for example, aggregates interact with each other and also interact with the binder. In this paper, we introduce different physical mechanisms to characterise the behaviour of the multi-phase compositions of mixtures. Based on these mechanisms, six compactability indices are proposed to characterise gyratory compaction curves. These indices are then used to evaluate the compactability of seven asphalt mixtures used in test sections constructed at the MnROAD research facility.

2. Physical mechanisms of compaction

Gyratory compaction of asphalt mixtures is performed under a combination of compression and shear forces. As shown in Figure 1, during gyratory compaction the asphalt mixture is confined in a cylindrical steel mould and is compressed by the external pressure P and gyratory sheared at an angle α. The direction of the shear is rotating at a rate of ω, called gyration rate. The deformation of material during gyratory compaction can be decomposed into the volumetric deformation and deviatoric deformation (distortion). The density change of materials is a result of the volumetric deformation, while density is conserved during pure distortion. The volumetric and deviatoric behaviours are often assumed to be uncoupled (Doll & Schweizerhof, 2000). However, this is not the case for the compaction of asphalt mixture, where the densification and distortion influence each other. On one hand, the density of mixture affects the stress needed to distort the mixture, namely its shear resistance: the shear resistance first increases and then decreases with the increase in density. On the other hand, the distortion also affects densification; in the gyratory compaction, the rate of densification increases with the increasing amplitude of distortion, which is the angle of gyration α (Prowell et al., 2003).

This coupling effect of densification and distortion originates from the material composition of asphalt mixture. In this study, two mesoscopic physical mechanisms are proposed to explain these

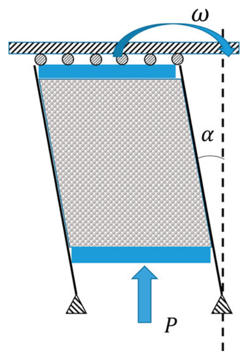

Figure 1. Sketch of gyratory compaction.

coupling effects, namely the effect of shear motion on densification process, and the effect of densification on shear resistance. The corresponding physical mechanisms proposed are the jamming of aggregates and the binder-aggregate interaction.

The jamming mechanism was first proposed and discussed in granular physics (Cates et al., 1998; Liu & Nagel, 1998). However, it has not been used before to investigate the compaction of asphalt mixtures. For this reason, we will first briefly introduce the original concept of jamming, and then describe how the jamming concept can be applied to the compaction process. Since the concept of jamming mechanism was originally proposed for dry granular systems (Cates et al., 1998; Liu & Nagel, 1998), it cannot fully explain compaction process, which also involves interstitial fluid like asphalt binder. Therefore, in this study we propose to consider another mechanism, namely the binder-aggregate interaction, to account for the effect of asphalt binder on compaction. By adding the binder-aggregate interaction, we extend the original jamming concept to granular-liquid systems, such as asphalt mixtures.

2.1. Jamming of aggregates

For granular materials, jamming of aggregates is believed to be the main physics responsible for the transition between the fluid-like and solid-like phase (Behringer & Chakraborty, 2019; Cates et al., 1998; Liu & Nagel, 1998). Granular materials, such as sand and aggregates, can flow under vibration or shear, but will jam to a certain state when the intensity of vibration or shear is lowered. A jammed state of aggregates is the state in which aggregates interlock with each other and cannot have any further movement under a static loading.

The jamming process can be illustrated by the jamming phase diagram (Liu & Nagel, 1998). As shown in Figure 2(a), jamming is affected by two factors, the volume fraction of aggregate (ϕ) and the shear resistance τ. The system of aggregates gets jammed when ϕ reaches a critical value ϕ_J. When $\phi > \phi_J$, the system can still get unjammed, by applying a shear force higher than the shear resistance. Note that, by considering the possibility of unjamming the system beyond the locking point, we can further explain the effect of shear on the densification process of compaction.

The jamming phase diagram is then used to explain the densification process during compaction. As shown in Figure 2(a), when $\phi < \phi_J$, the state represented by point A, the aggregates are separated from each other, and the system can be easily deformed with zero shear resistance, which corresponds to the fluid-like phase. If a static pressure is applied to reduce the total volume of the system, ϕ will increase and reach the critical volume fraction ϕ_J that represents the beginning of the jammed phase. Once ϕ_J is reached (point B), aggregates become jammed, and cannot be further densified by pure static compression. Therefore, ϕ_J represents the maximum volume fraction of aggregates that the system can reach under static compression.

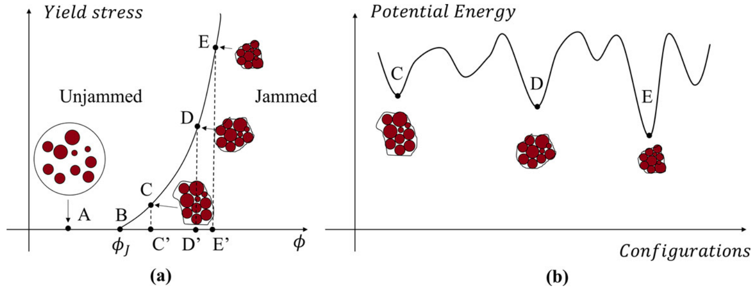

Figure 2. (a) Jamming phase diagram, (b) potential energy of different configurations.

Once the aggregates are jammed, the system starts to develop shear resistance. To further densify the material, external excitations, such as shear or vibration, need to be applied to overcome the shear resistance to unjam the system, and enable it to evolve to a denser state. This is shown in Figure 2(a): the system evolves from point C to D, and then to E. If the system is at a state represented by point C′, a jammed state, it cannot evolve to the denser state D′ through the line C′→D′ directly. Instead, the feasible path is C′→C→D→D′, which means that, in order to evolve to point D, the jammed state C′ is first unjammed to state C by applying excitations to overcome shear resistance.

The jamming mechanism can also be understood from the analysis of the energy landscape (Charbonneau et al., 2014), which is also applicable to the compaction of asphalt mixtures For a system of aggregates, the potential energy provided by the static compression decreases as the volume of the system decreases. Therefore, potential energy decreases with the increase in volume fraction of aggregates ϕ, as shown in Figure 2(b). If aggregates are free to move and rearrange, the whole system tends to evolve to the state with a lower potential energy, which is also corresponding to the densest state of aggregate packing (greatest ϕ). Each jammed state of aggregates represents a local minimum of the potential energy, as shown in Figure 2(b). Under pure static compression, without external excitations, the system is trapped in that local minimum state. If external shear or vibration is applied, the external energy enables the system to overcome the energy barrier (i.e. enable the aggregates to unjam so that they can rearrange) and move to configurations with lower energy states, which correspond to denser and denser packing states of aggregates. The transition from C to D and E in Figure 2(b) exemplifies this process.

Based on the physical mechanism of jamming, the densification process of compaction can be viewed as the evolving of jammed states of aggregates under the excitation of shear (e.g. laboratory gyratory compaction) or vibration (e.g. vibration roller compaction in the field).

2.2. Binder-aggregate interaction

The physical mechanism of aggregate jamming explains the effect of shear on densification process, but it cannot fully explain the evolution of shear resistance during compaction. As shown in Figure 2(a), jamming mechanism alone predicts that the shear resistance increases as the density increases. However, as shown by the experimental data of this study and other studies (Faheem & Bahia, 2004; Guler et al., 2000; Shamsi & Mohammad, 2010; Stakston & Bahia, 2003), the shear resistance in gyratory compaction first increases but then decreases with increase in density. In this study, we postulate that the decrease in shear resistance of mixture during the latter part of compaction is caused by the binder-aggregate interaction.

To explain the interaction between aggregates and binder, we adopt the pore pressure and effective stress concepts from the critical state theory in soil mechanics (Schofield & Wroth, 1968). Similar to the role of water in soil, binder in the mixture can also develop pore pressure when most of air voids are extruded out (when ϕ reaches a certain level). The total stress is the sum of effective stress from

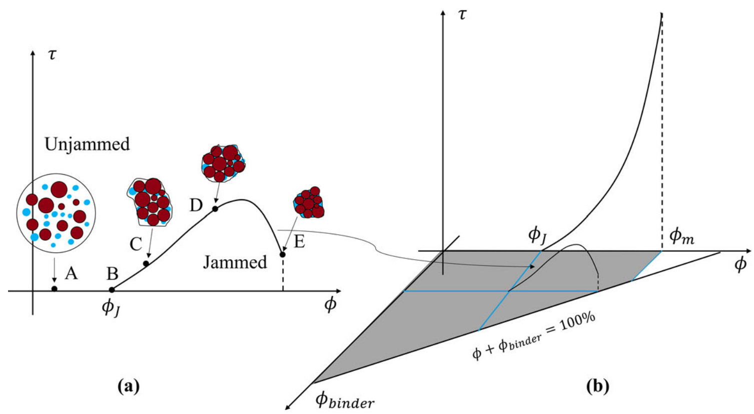

Figure 3. (a) Jamming Phase diagram of mixture with a fixed binder content, (b) generalised Jamming phase diagram of the aggregates binder system.

the solid contact of aggregates and the pore pressure in the liquid binder, i.e.:

$$p = p_{eff} + p_{pore} \tag{1}$$

where p is the total stress; p_{eff} is the effective stress; p_{pore} is the pore pressure.

At a constant p, an increase in p_{pore} leads to a decrease in p_{eff}. The shear resistance of granular materials depends on the friction between their constituent particles, and the friction is proportional to p_{eff} (Schofield & Wroth, 1968). The pore pressure p_{pore} of binder does not contribute to friction, since the binder serves as lubricant in the aggregate-binder system.

We now explain the compaction process of asphalt mixtures by combining the mechanisms of jamming and aggregate-binder interaction. A schematic jamming phase diagram for asphalt mixtures with a certain binder content can be sketched in Figure 3(a). At the beginning of the compaction process, the mixture is in a relatively loose state, e.g. point C. When the mixture is compressed, the binder can flow to occupy the space in air voids, and pore pressure cannot develop. In the latter phase of compaction, e.g. point D, space in air voids has decreased considerably, and the binder has no space to flow and therefore p_{pore} increases. Since the total stress is kept constant during compaction, p_{eff} decreases accordingly, which therefore, causes the decrease of shear resistance.

It should be noted that Figure 3(a) differs from Figure 2(a) because of the binder-aggregate interaction. Since the interaction between aggregates and binder becomes more evident as the binder content increasing, the binder content should be considered as another parameter for the jamming phase diagram of an aggregate-binder system. We therefore propose a more general phase diagram for aggregate-binder system as sketched in Figure 3(b), in which the third axis, the volume fraction of binder (ϕ_{binder}), is added. As shown, when $\phi_{binder} = 0\%$, there is no aggregate binder interaction, so the ϕ–τ relationship returns to that shown in Figure 2(a), whereas for a certain amount of binder content ϕ_{binder}, due to the aggregate binder interaction, the ϕ-τ relationship becomes that shown in Figure 3(a). More generally, τ can be viewed as a function of both ϕ and ϕ_{binder} and can be represented by a surface in the τ-ϕ-ϕ_{binder} coordinates.

The feasible domain of ϕ and ϕ_{binder} has to satisfy three additional constrains listed in Equation (2).

$$\begin{cases} 0\% < \phi < \phi_m \\ 0\% < \phi_{binder} < 100\% \\ \phi + \phi_{binder} < 100\% \end{cases} \tag{2}$$

The first inequality says that ϕ is bounded by 0% and the maximum volume fraction ϕ_m corresponding to the closest packing of aggregates. The second one says that ϕ_{binder} is bounded by 0% and 100%.

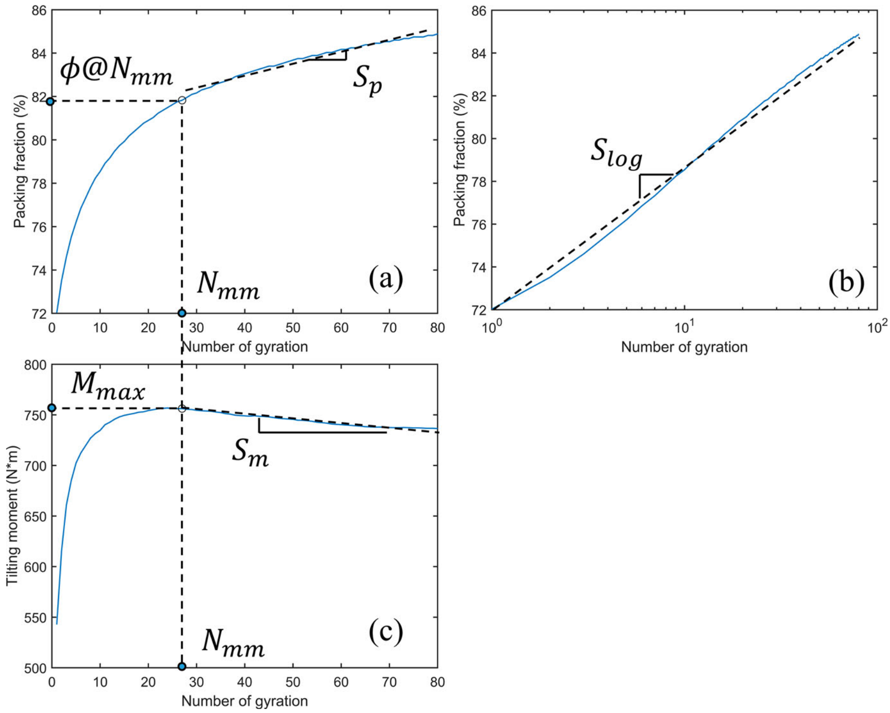

Figure 4. Typical compaction curves, (a) densification curve, (b) semi-logarithmic densification curve, (c) shear resistance curve.

The third one says that the volume fraction of binder plus aggregates cannot exceed 100%. Based on these three inequalities, the feasible domain is marked as the grey trapezoid region in Figure 3(b).

Drawing an analogy with soil consolidation, for gyratory compaction of asphalt mixture the condition can be viewed as undrained, since material is confined in the steel mould. Even for field compaction, where there is no real confinement, due to the high viscosity of the binder, the time scale for binder to drain out is very large compared to the speed of the compaction. Therefore, the proposed mechanism of binder-aggregate interaction is applicable to both laboratory gyratory compaction and field compaction.

3. Interpretation of gyratory compaction curves and Mechanism-Based compactability indices

The two physical mechanisms proposed in the previous section are now used to interpret gyratory compaction curves. Compaction data, obtained from a typical gyratory compaction test, is used in Figure 4(a–c) for this purpose.

Figure 4(a) shows the densification process that takes place during compaction. In order to emphasise the role of the jamming process, the volume fraction of aggregate ϕ is chosen as the *y*-axis, instead of the commonly used $\%G_{mm}$ (percentage of the theoretical maximum specific gravity).

Figure 4(c) shows the change of shear resistance with number of gyration. The shear resistance of the mixture is evaluated by the tilting moment, measured during gyratory compaction using the Gyratory Load Plate Assembly (GLPA) of the Pine G2 gyratory compactor. The GLPA has three load cells from which the eccentric moment of the static pressure on the upper loading plate can be measured. This eccentric moment is called the tilting moment (Guler et al., 2000). The tilting moment measures the moment needed for shearing the mixture to a fixed angle, the angle of gyration. Therefore, the tilting moment can serve as a good representation of the shear resistance of mixtures.

As shown in Figure 4(c), the shear resistance reaches its maximum at a certain number of gyrations, then starts to decrease. This phenomenon of the maximum shear resistance was first studied by Guler et al. (2000) and was considered as an indication of unstable mixtures. In a later study, Shamsi and Mohammad (2010) showed that the number of gyrations at which the shear resistance was maximum had a high correlation with the traditional locking point, which implies that a certain degree of locking may have already formed. However, no explanation was given for why there is a maximum shear resistance as the density increases.

This phenomenon can be explained by the proposed physical mechanisms. The increase in the shear resistance at the beginning of compaction is a result of the aggregate jamming, in which the shear resistance increases with an increasing volume fraction of aggregates ϕ, as shown in Figure 2(a). The decrease in the shear resistance in the later part of compaction is a result of binder-aggregate interaction. As ϕ increase, at a certain point, the increase in pore pressure of binder will cause a reduction of the effective stress p_{eff} in aggregates and therefore reduces the shear resistance of mixture.

Figure 4(b) presents the same data as Figure 4(a) but in the semi-logarithmic scale. As shown, N and ϕ exhibit an approximately linear relationship in the semi-logarithmic scale plot, which confirms the results of Moutier (1974).

Based on this interpretation of gyratory compaction curves, the following indices are proposed to evaluate the compactability of mixtures:

(1) N_{mm}: the number of gyrations, corresponding to the maximum tilting moment.
(2) M_{max}: the maximum tilting moment, corresponding to the maximum shear resistance.
(3) ϕ_{mm}: packing fraction at N_{mm}.
(4) S_p: the slope of the linear least squares regression of ϕ versus N, for $N > N_{mm}$ which characterises the rate of evolution of jammed states or the rate of densification, after N_{mm} is reached.
(5) S_m: the slope of the linear least squares regression of the tilting moment versus N, for $N > N_{mm}$ which characterises the decreasing rate of shear resistance, after N_{mm} is reached.
(6) S_{log}, the slope of the linear least squares regression of ϕ versus log$N$, which characterises the rate of densification.

These proposed indices provide a more detailed characterisation of the compaction process, including the characterisation of both the densification process and the change of shear resistance. Since the proposed indices are anchored by the physical mechanisms, they are expected to exhibit better correlations with material compositions. It is important to note that the proposed indices cannot be obtained for dry aggregate systems, for which a critical gyratory number N_{mm} does not exists.

4. Material composition of MnROAD asphalt mixtures

A statistical analysis is performed next to investigate how the material composition of the asphalt mixture, such as binder content and aggregate gradation, relate to the proposed compactability indices.

4.1. Material information

Seven asphalt mixtures, used in the construction of test sections at MnROAD in 2016, were selected for the analysis. Detailed information is shown in Table 1. The composition is presented in terms of weight percentages. RAP_AC denotes the asphalt binder contribution from recycled asphalt pavements (RAP), and RAS_AC denotes the asphalt binder contribution from recycled asphalt shingles (RAS). RAC represents the total Reclaimed Asphalt Binder Content, which includes both RAP and RAS. No rejuvenators were used in these mixtures.

The aggregates used to make the seven mixtures come from similar sources, and therefore, they have similar properties. The coarse aggregate angularity is 98% (percentage of at least two fractured

Table 1. Mixture information

Mixture ID	Mix 1	Mix 2	Mix 3	Mix 4	Mix 5	Mix 6	Mix 7
Cell Number	Cell 16	Cell 17	Cell 18	Cell 19	Cell 20	Cell 21	Cell 23
Binder PG	64S-22	64S-22	64S-22	64S-22	52S-34	58H-34	64E-34
% RAP	20	10	20	20	30	20	15
% RAS	5	5	0	0	0	0	0
% RAP_AC	1.23	0.62	1.23	1.23	1.85	1.23	0.92
% RAS_AC	0.87	0.87	0.00	0.00	0.00	0.00	0.00
% RAC	2.10	1.49	1.23	1.23	1.85	1.23	0.92
% Total AC	5.27	5.43	5.43	5.70	5.32	5.38	5.23

Table 2. Aggregate gradation of mixtures.

	Percent Passing (%)						
Sieve size, mm	Mix 1	Mix 2	Mix 3	Mix 4	Mix 5	Mix 6	Mix 7
19	100	100	100	100	100	100	100
12.5	93.9	93.1	93.7	93.7	93.3	93.7	93.1
9.5	83.1	81.1	82.7	82.7	81.4	82.7	81
6.25	68.0	65.2	67.4	68.3	66.0	67.4	64.3
4.75	61	57.9	60.4	61.6	58.9	60.4	56.6
2.36	45.5	42.2	43.5	45.3	43.7	43.5	39.8
1.18	32.5	29.9	30.8	31.5	31	30.8	28.1
0.6	22	20.3	21	20.7	20.7	21	19.3
0.3	13.3	12.7	12.8	11.8	11.9	12.3	12
0.15	8	7.8	7.6	6.5	6.7	7.6	7.3
0.075	5.3	5.2	5	4.1	4.3	5	4.9

faces). The fine aggregate angularity is 47% (fine aggregate packing fraction). The percentage of flat and elongated particles (dimensional ratio larger than 5:1) is 3%. The only difference in aggregate properties of these mixtures is the aggregate gradation.

4.2. Aggregate gradation analysis

The gradations of the aggregates are listed in Table 2. The mixtures share the same nominal maximum aggregate size (NMAS), which is 12.5 mm.

The Bailey method and distance from the maximum density line are used to characterise aggregates gradation. The Bailey method is an empirical method for selecting and adjusting aggregate gradation in mixture design (Vavrik et al., 2002). Studies have shown that the Bailey method parameters are strongly correlated with the compactability of mixtures (Graziani et al., 2012; Leiva & West, 2008).

In the Bailey method, three critical sieve sizes are defined. The first is the Primary Control Sieve (PCS), which separates the coarse and fine aggregates. The PCS is defined as the closest sieve to 0.22 × NMAS. Similarly, the Secondary Control Sieve (SCS) is defined as the closest sieve to 0.22 × PCS, and the Tertiary Control Sieve (TCS) is defined as the closest sieve to 0.22 × SCS. The passing percentage of PCS (%PCS) shows the overall fineness of the blend. The larger the %PCS, the finer the blend.

Three ratios of passing percentage are defined to characterise the gradation at different scales. Coarse Aggregate ratio (CA) is defined as Equation (3), to characterise the gradation of coarse aggregates. Similarly, Fine Aggregate Coarse ratio (FA_c) and Fine Aggregate fine ratio (FA_f) are defined as Equations (4) and (5), to characterise the gradation of the coarse portion and fine portion fine aggregates, respectively.

$$CA = \frac{(\%\text{Half Sieve} - \%\text{PCS})}{(100\% - \%\text{Half Sieve})} \tag{3}$$

Table 3. Parameters to characterise gradation

Mixture ID	Mix 1	Mix 2	Mix 3	Mix 4	Mix 5	Mix 6	Mix 7
% PCS	48.4	48.1	48.3	45.7	47.4	48.3	48.5
CA Ratio	0.808	0.780	0.772	0.783	0.811	0.772	0.752
FA_c Ratio	0.364	0.384	0.362	0.314	0.324	0.362	0.378
d_{MDL}	55.3	41.6	50.3	58.2	48.9	50.8	38.7

$$FA_c = \frac{\%SCS}{\%PCS} \tag{4}$$

$$FA_f = \frac{\%TCS}{\%SCS} \tag{5}$$

where '%' before the critical sieve sizes meaning the passing percentage of the corresponding sieve. As the CA, FA_c, or FA_f increases, the corresponding portion of the aggregates becomes finer.

Compactability of mixtures is also related to how close the gradation curve is to the maximum density line (MDL) (Hekmatfar et al., 2015; Huber et al., 2016). The MDL is defined as a power-law gradation curve, i.e. %Passing of sieve size $D_i = 100 \times \left(\frac{D_i}{D_{max}}\right)^n$, where D_{max} is the maximum aggregate size and $n = 0.45$ (Fuller & Thomson, 1907; Sánchez-Leal, 2007). The MDL on the 0.45 power gradation chart is represented by a straight diagonal line (Mamlouk & Zaniewski, 2016). Therefore, we define another parameter called the distance to MDL (d_{MDL}), which is calculated as the sum of the absolute difference between the gradation curve and MDL at each sieve size:.

$$d_{MDL} = \sum_{i=1}^{number\ of\ sieves} \left| \%Passing\ of\ sieve\ i - 100 \times \left(\frac{D_i}{D_{max}}\right)^{0.45} \right| \tag{6}$$

The calculated Bailey method parameters and d_{MDL} for the seven mixtures are summarised in Table 3.

It is important to note that the seven mixtures studied are fine-graded, and the critical sieve sizes had to be adjusted (Vavrik et al., 2002). All critical sieve sizes are scaled down by a factor of 0.22. FA_f cannot be calculated since, after the adjustment, the new TCS becomes too small (less than 0.075 mm).

5. Compactability evaluation of MnROAD mixtures

Gyratory compaction tests of the seven mixtures were conducted during the mix design phase, according to AASHTO T312 (2019). The compaction temperature was determined based on the equiviscous principle (Yildirim et al., 2006), and varied with the asphalt binder PG. For the seven mixtures studied, the compaction temperature ranged from 123 to 143 °C. The external pressure P is 600 kPa, the gyration angle α is 1.16°, and the rate of gyration ω is 30 gyrations per minute. Specimen diameter was 150 mm and the height was 115 ± 5 mm after compaction. For each mixture, gyratory compactions were conducted at three levels of total asphalt binder content, 5.0%, 5.5%, and 6.0% (for Mix 3 only, the total binder content was 4.8%, 5.3%, and 5.8%, respectively). For each level of total asphalt binder content, two or three replicates were compacted, for a total of 48 gyratory compaction tests. An example of compaction curves for Mix 1 is shown in Figure 5. The points corresponding to N_{mm} are identified by circles.

As seen in Figure 5(a), the replicates with higher total binder content are more compactable, since at a same gyration number, they have a higher packing fraction of aggregates. As seen in Figure 5(b), the mixtures with the highest total binder content (6%) have a higher decreasing rate of tilting moment (S_m) after reaching N_{mm}. The compaction curves of all other mixtures exhibit similar trends, and are not shown. Based on the compaction curves, the physical indices are computed and listed in Table 4.

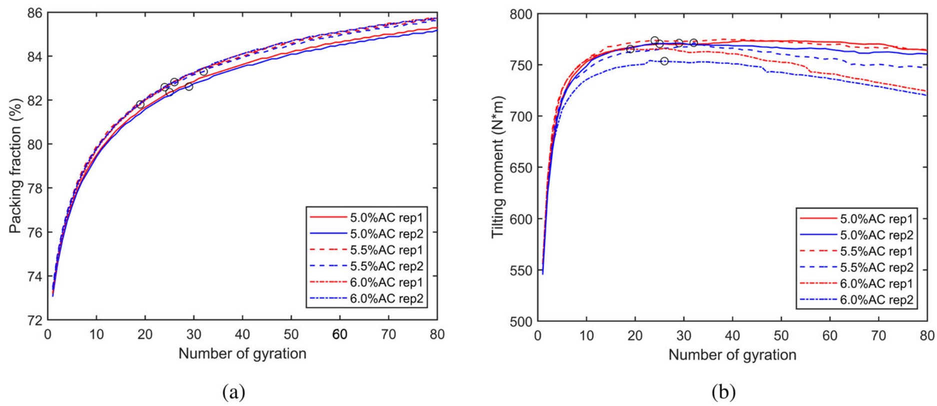

Figure 5. The compaction curves of Mix 1. (a): the densification curve; (b): the shear resistance curve. Note: the circles identifies N_{mm}, when shear resistance is maximum

Table 4. Compactability indices of different mixtures

	%AC	N_{mm}	$\Phi@N_{mm}$	M_{max}	S_p	S_m	S_{log}
Mix1	5	27.0	82.48	770.8	0.0519	−0.163	7.376
	5.5	28.0	82.94	772.6	0.0518	−0.345	7.493
	6	22.5	82.31	759.4	0.0591	−0.651	7.837
Mix2	5	26.5	81.79	759.6	0.0569	−0.322	7.819
	5.5	18.7	80.96	768.1	0.0665	−0.326	7.683
	6	24.3	81.91	776.9	0.0601	−0.522	8.108
Mix3	4.8	20.5	80.42	738.5	0.0611	−0.133	7.206
	5.3	22.0	81.76	768.8	0.0598	−0.320	7.507
	5.8	14.0	80.26	767.7	0.0788	−0.328	8.003
Mix4	5	22.0	81.07	802.5	0.0468	−0.304	6.909
	5.5	19.5	80.62	824.6	0.0542	−0.488	7.270
	6	22.0	81.68	858.6	0.0505	−0.609	7.522
Mix5	5	37.3	83.08	800.9	0.0441	−0.203	7.091
	5.5	11.0	79.98	858.1	0.0804	−0.240	7.495
	6	16.0	81.37	860.6	0.0673	−1.206	7.468
Mix6	5	37.3	82.81	770.5	0.0485	−0.093	7.697
	5.5	29.5	82.57	772.7	0.0564	−0.189	7.953
	6	23.7	82.06	767.5	0.0629	−0.419	8.194
Mix7	5	22.0	81.73	747.4	0.0628	−0.149	7.864
	5.5	25.0	82.35	738.9	0.0604	−0.368	8.128
	6	18.0	81.05	735.1	0.0712	−0.667	8.379

6. Correlations between mixture properties and compactability indices

A statistical analysis is conducted to identify correlations between mixtures' material properties and the proposed compactability indices. The investigated material properties include:

(1). total binder content (%AC),
(2). reclaimed binder content (%RAC),
(3). Bailey method parameters (%PCS, CA, and FA_c), and
(4). distance to the maximum density line (d_{MDL}).

Although the viscosity of binder has a profound influence on the compaction process, it is not investigated in this study since the gyratory compaction tests are conducted at temperatures at which the binders have similar viscosities (Yildirim et al., 2006). Meanwhile, the shape and angularity of aggregates are also not considered in this study since similar aggregate sources were used to prepare the mixtures. The focus of this study is on the effects of asphalt binder content and aggregate gradation on compaction.

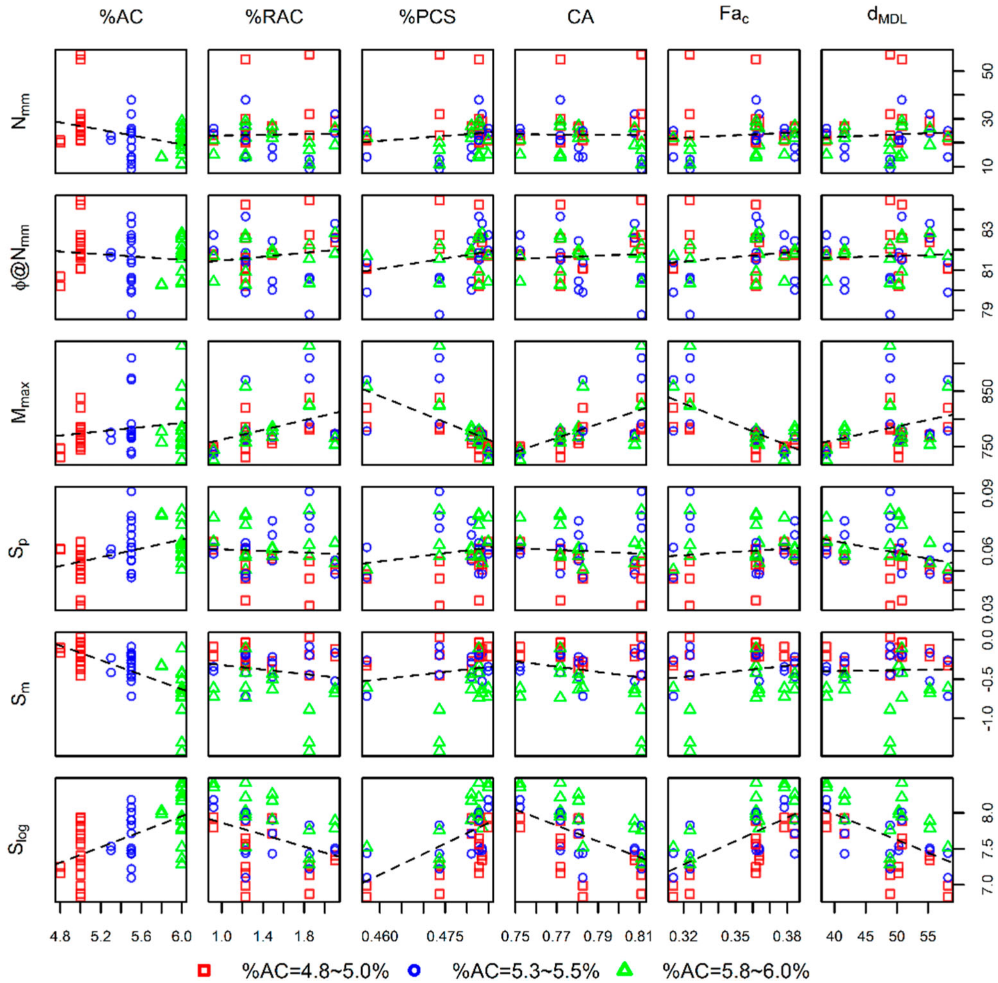

Figure 6. Scatter plots between mixture properties and compactability indices.

First, a correlation analysis is conducted to identify high correlation pairs. Then, multiple linear regression models for each compactability index are obtained using the best subset regression method.

6.1. Correlation analysis

Scatter plots of mixtures properties (horizontal axis) versus the compactability indices (vertical axis) are shown in Figure 6. The data is divided into three groups according to the total binder content.

In the correlation analysis, the Pearson correlation coefficients, r, and p-value are computed. The p-value is used for the hypothesis test which checks the statistical significance of the linear correlation. The null hypothesis is "the correlation coefficient is not significantly different from 0". If the p-value is less than the significance level (0.05), we can reject the null hypothesis, and conclude the linear correlation is statistically significant. Otherwise, we accept the null hypothesis. The calculated r and p-value are listed in Table 5. Pairs that passed the hypothesis test (p-value < 0.05) are identified in bold in Table 5.

For each of the correlated pairs, we examine whether the correlation can be explained by the proposed physical mechanisms. It is observed that the total binder content (%AC) has the most

Table 5. Results of pairwise correlation analysis.

	%AC	%RAC	%PCS	CA	FA_c	d_{MDL}
N_{mm}	$\mathbf{p = 0.01}$ $\mathbf{r = -0.35}$	$p = 0.85$ $r = 0.03$	$p = 0.39$ $r = 0.13$	$p = 0.94$ $r = -0.01$	$p = 0.54$ $r = 0.09$	$p = 0.63$ $r = 0.07$
$\phi@N_{mm}$	$p = 0.39$ $r = -0.13$	$p = 0.29$ $r = 0.16$	$p = 0.09$ $r = 0.25$	$p = 0.66$ $r = 0.07$	$p = 0.27$ $r = 0.16$	$p = 0.75$ $r = 0.05$
M_{max}	$p = 0.23$ $r = 0.18$	$\mathbf{p = 0.01}$ $\mathbf{r = 0.37}$	$\mathbf{p < 0.01}$ $\mathbf{r = -0.60}$	$\mathbf{p < 0.01}$ $\mathbf{r = 0.57}$	$\mathbf{p < 0.01}$ $\mathbf{r = -0.71}$	$\mathbf{p = 0.02}$ $\mathbf{r = 0.34}$
S_p	$\mathbf{p < 0.01}$ $\mathbf{r = 0.41}$	$p = 0.65$ $r = -0.07$	$p = 0.16$ $r = 0.20$	$p = 0.60$ $r = -0.08$	$p = 0.41$ $r = 0.12$	$\mathbf{p = 0.03}$ $\mathbf{r = -0.32}$
S_m	$\mathbf{p < 0.01}$ $\mathbf{r = -0.65}$	$p = 0.23$ $r = -0.18$	$p = 0.23$ $r = 0.18$	$p = 0.13$ $r = -0.22$	$p = 0.19$ $r = 0.19$	$p = 0.87$ $r = 0.02$
S_{log}	$\mathbf{p < 0.01}$ $\mathbf{r = 0.55}$	$\mathbf{p = 0.01}$ $\mathbf{r = -0.38}$	$\mathbf{p < 0.01}$ $\mathbf{r = 0.59}$	$\mathbf{p < 0.01}$ $\mathbf{r = -0.54}$	$\mathbf{p < 0.01}$ $\mathbf{r = 0.66}$	$\mathbf{p < 0.01}$ $\mathbf{r = -0.54}$

Note: The boldfaced cells have p-value < 0.05, which indicates the linear correlation is statistically significant.

significant effect on compactability; it is correlated with most compactability indices, including N_{mm}, S_p, S_m, and S_{log}. The negative correlations of %AC with N_{mm} and S_m is reasonable from the viewpoint of binder-aggregate interaction. It is easier for mixtures to develop pore pressure when the binder content is higher, which causes a fewer number of gyration (N_{mm}) before reaching the peak shear resistance, and a faster dropping rate (S_m) of shear resistance when $N > N_{mm}$.

The positive correlations of %AC with S_p and S_{log} indicate that the increase of total binder content accelerates the densification process. These can also be explained using the proposed mechanisms; asphalt binder acts as the interstitial fluid that provides the lubrication between aggregates, and makes it easier for the jammed state to unjam by shear, and increases the rate of evolving from one jammed state to another.

The reclaimed binder content (%RAC) has a positive correlation with M_{max} and a negative correlation with S_{log}, which indicates that %RAC has an adverse effect on compaction, because it tends to increase shear resistance and decrease densification rate. These correlations are reasonable because, compared to virgin binder, reclaimed binder has higher viscosity and less lubricated which have adverse impacts on compaction.

The Bailey parameters are correlated with M_{max} and S_{log}. The results of %PCS shows that the increase in the proportion of fine aggregates (the increase in %PCS) decreases the maximum shear resistance (M_{max}), and increases the overall densification rate (S_{log}). The result shows that the increase in the fineness of the coarse portion of aggregates (the increase in the CA) leads to an increase in the maximum shear resistance (M_{max}), and a decrease in the overall densification rate (S_{log}). The results of FA_c indicate that the increase in the fineness of the fine portion of aggregates (the increase in FA_c) causes a decrease in the maximum shear resistance (M_{max}), and an increase in the overall densification rate (S_{log}). The results of %PCS and FA_c are consistent with practical experiences that the compactability of mixtures increase with the increase in the fineness of aggregates. However, the results of CA suggest that the coarseness of the coarse portion of aggregates would improve the compactability.

The distance to the maximum density linear, d_{MDL}, is correlated to M_{max}, S_{log}, and S_p. A reduction in d_{MDL} helps compaction, since it decreases the maximum shear resistance (M_{max}), and increase the rate of densification (S_{log} and S_p).

The identified correlations between compactability and aggregate gradation, including the Bailey parameters and d_{MDL}, can be reasonably explained by the physical mechanism of jamming. It is clear that different gradation will lead to different critical volume fraction ϕ_J and maximum dense packing fraction ϕ_m of jamming. Higher ϕ_J and ϕ_m are corresponding to higher compactability of mixtures. However, how exactly ϕ_J and ϕ_m are affected by gradation is not clear. Therefore, more research is needed to reveal this relationship.

Table 6. Best subset regression for S_{log}.

Size of subset	%AC	%RAC	%PCS	CA	FA_c	d_{MDL}	Adj. R^2
1					√		0.423
2	√				√		0.688
3	√		√	√			0.771
4	√		√	√		√	**0.773**
5	√		√	√	√	√	0.771
6	√	√	√	√	√	√	0.766

Note: The highest adjusted R^2 is boldfaced.

Table 7. Results of multiple linear regressions.

Compactability indices	Best subset regression model	Adj. R^2	R^2
N_{mm}	$N_{mm} = 65.4 - 7.7 \times \%AC$	0.104	0.123
$\phi@N_{mm}$	$\phi@N_{mm} = 65.3 + 34.2 \times \%PCS$	0.041	0.062
M_{max}	$M_{max} = 800.7 + 666.7 \times CA - 1264.1 \times FA_c - 1.86 \times d_{MDL}$	0.616	0.640
S_p	$S_p = 0.0276 + 0.0107 \times \%AC - 0.000538 \times d_{MDL}$	0.212	0.245
S_m	$S_m = 2.153 - 0.464 \times \%AC$	0.410	0.422
S_{log}	$S_{log} = 2.23 + 0.524 \times \%AC + 19.0 \times \%PCS - 7.89 \times CA - 0.00723 \times d_{MDL}$	0.773	0.793

6.2. Multiple linear regression

Multiple linear regression models are used to quantify the effect of each material property on the compactability indices, and to consider the joint effect between different material properties.

As shown in the correlation analysis, for a compactability index, not all material properties have a significant correlation with it. Therefore, inclusion of all the six material properties as predictors will over fit the compactability index. A predictor selection process is conducted to identify the best subset of all material properties.

The best subset selection method (Friedman et al., 2001) is adopted to perform a predictor selection. In this study, there are 6 material properties, so the subset can have a size ranges from 1 to 6. For a certain size k, the best subset selection method finds the subset of k predictors that produces the best fit in terms of the coefficient of determination, R^2. The best subsets of different k are then compared by the adjusted R^2. The subset that produces the highest adjusted R^2 is chosen as the final best subset. The adjusted R^2 compares the explanatory power of regression models that contain different numbers of predictors. It is a modified version of R^2 that has been adjusted for the number of predictors in the model (Weisberg, 2014).

Table 5 exemplifies the best subset selection process for S_{log}. For each subset size, the best subset is identified and marked in Table 6. Among different sizes of subset, it is found that, when size $= 4$, adjusted R^2 gets its maximum (0.773). Therefore, the corresponding subset, containing 4 predictors (%AC, %PCS, CA, and d_{MDL}), is identified as best subset for the multiple linear regression model of S_{log}.

The same approach is applied for the other compactability indices, and the best linear regression models of each compactability index are summarised in Table 7.

R^2 is a goodness-of-fit measure of the regression model. As shown in Table 7, the values of R^2 of the regression models are relatively low (less than 0.8). This is expected given the intrinsic randomness of asphalt mixture as a heterogeneous material. Other factors, such as the shape and texture of aggregates, which were not captured in this study, also influence this randomness. Also, the regression models only considered the linear case while higher orders (nonlinear) correlations were ignored, which could be another reason for the low value of R^2.

As shown in Table 7, the regression models for M_{max} and S_{log} have reasonable R^2s (0.640 and 0.793 respectively), considering the intrinsic randomness. These models quantify the effect of material properties on compactability, thus will be helpful for mixture design. The compactability of mixtures can be controlled in design phase by determine the criteria for M_{max} and S_{log}. Then, these formulas can help determine or adjust the material properties.

For the regression models of other compactability indices, the R^2s are too low (less than 0.422). It implies that the six material properties selected are not capable to fully explain these compactability indices. To improve the performance of these models, other material properties need to be further considered, e.g. the shape and angularity of aggregate, and the rheology of binder and fine aggregate matrix (FAM).

7. Conclusions

In this paper, two physical mechanisms, jamming of aggregates and aggregate binder interaction, were proposed to explain the compaction process of asphalt mixture. Based on these mechanisms, six compactability indices were developed to characterise the gyratory compaction data and to evaluate the compactability of seven mixtures from MnROAD. Correlations between compactability and material properties, such as binder content and gradation, were analysed. The following conclusions were drawn from this study.

- Using the physical mechanism of aggregates jamming, compaction process of asphalt mixture can be interpreted as the evolving of jammed states of aggregates under the excitation of shear or vibration. This interpretation explains why shear and vibration enhance densification, and why shear resistance increases with density, showing the coupling effects between shear and densification process of asphalt mixture.
- The physical mechanism of binder-aggregate interaction explains the decrease in shear resistance for the later stage of gyratory compaction.
- The statistical analysis identified several correlations between the compactability indices and the material properties. The identified correlations can be well explained by the physical mechanisms, which, offers support to the validity of the proposed mechanisms.
- The identified correlations between the compactability indices and aggregate gradation were not fully understood. The correlations can be attributed to the effects of aggregate gradation on the critical volume fractions of the aggregate jamming, ϕ_J and ϕ_m. However, further research is needed to better understand how ϕ_J and ϕ_m are affected by aggregate gradation.
- Multiple linear regression models for each compactability indices were developed using material properties. Potentially, the models can be used in mixture design to control the compactability of mixtures.

Due to the limited number of mixtures studied, the multiple linear regression models developed may not be applicable for all mixtures. A larger set of mixtures needs to be further studied to consider a wider range of material properties in the regression models, such as aggregate shape, angularity, and binder rheology. This study provides a general approach to evaluate the compactability of mixtures and design denser mixtures that can significantly improve the durability of asphalt pavements.

Acknowledgments

The authors gratefully acknowledge the financial support provided by the Minnesota Department of Transportation and Local Road Research Board. The authors also acknowledge NCAT for providing the compaction data used in this study.

Disclosure statement

No potential conflict of interest was reported by the author(s).

Funding

This work was supported by Minnesota Department of Transportation: [Grant Number 1003325 WO#106].

ORCID

Tianhao Yan http://orcid.org/0000-0003-0706-3189
Mihai O. Marasteanu http://orcid.org/0000-0001-8331-4504
Jia-Liang Le http://orcid.org/0000-0002-9494-666X

References

AASHTO R35. (2017). *Standard practice for Superpave volumetric design for asphalt mixtures*. American Association of State Highway and Transportation Officials.

AASHTO T312. (2019). *Standard method of test for preparing and determining the density of asphalt mixture specimens by means of the Superpave Gyratory compactor*. American Association of State Highway and Transportation Officials.

Behringer, R. P., & Chakraborty, B. (2019). The physics of jamming for granular materials: A review. *Reports on Progress in Physics*, *82*(1), 012601. https://doi.org/10.1088/1361-6633/aadc3c

Brown, E. R., Hainin, M. R., Cooley, L. A., & Hurley, G. (2004). *NCHRP report 531: Relationship of air voids, lift thickness, and permeability in Hot Mix asphalt pavements*. Transportation Research Board. National Research Council.

Cates, M. E., Wittmer, J. P., Bouchaud, J. P., & Claudin, P. (1998). Jamming, force chains, and fragile matter. *Physical Review Letters*, *81*(9), 1841–1844. https://doi.org/10.1103/PhysRevLett.81.1841

Charbonneau, P., Kurchan, J., Parisi, G., Urbani, P., & Zamponi, F. (2014). Fractal free energy landscapes in structural glasses. *Nature Communications*, *5*(1), 1–6. https://doi.org/10.1038/ncomms4725

Dessouky, S., Masad, E., & Bayomy, F. (2004). Prediction of hot mix asphalt stability using the superpave gyratory compactor. *Journal of Materials in Civil Engineering*, *16*(6), 578–587. https://doi.org/10.1061/(ASCE)0899-1561(2004)16:6(578)

Doll, S., & Schweizerhof, K. (2000). On the development of volumetric strain energy functions. *Journal of Applied Mechanics*, *67*(March), 17–21. https://doi.org/10.1115/1.321146

Faheem, A. F., & Bahia, H. U. (2004). *Using the gyratory compactor to measure the mechanical stability of asphalt mixtures*. Wisconsin Highway Research Program. http://digital.library.wisc.edu/1793/6907.

Finn, F. N., & Epps, J. A. (1980). *Compaction of hot mix asphalt concrete*. Texas Transportation Institute, the Texas A & M University System.

Friedman, J., Hastie, T., & Tibshirani, R. (2001). *The elements of statistical learning* (Vol. 1, No. 10). Springer series in statistics.

Fuller, W., & Thomson, S. (1907). *The laws of proportioning concrete*. *Transactions of the American Society of Civil Engineers*, *LIX*, *59*(2), 67–143. https://doi.org/10.1061/TACEAT.0001979

Graziani, A., Ferrotti, G., Pasquini, E., & Canestrari, F. (2012). An application to the European practice of the Bailey method for HMA aggregate grading design. *Procedia-Social and Behavioral Sciences*, *53*, 990–999. https://doi.org/10.1016/j.sbspro.2012.09.948

Guler, M., Bahia, H. U., Bosscher, P. J., & Plesha, M. E. (2000). Device for measuring shear resistance of hot-mix asphalt in gyratory compactor. *Transportation Research Record*, *1723*(1), 116–124. https://doi.org/10.3141/1723-15

Harmelink, D. S., & Aschenbrener, T. (2002). *In-place voids monitoring of hot mix asphalt pavements* (No. CDOT-DTD-R-2002-11,). Colorado Department of Transportation, Research Branch.

Hekmatfar, A., McDaniel, R. S., Shah, A., & Haddock, J. E. (2015). *Optimizing laboratory mixture design as It relates to field compaction to improve asphalt mixture durability (joint Transportation Research Program publication No. FHWA/IN/JTRP-2015/25)*. Purdue University. https://doi.org/10.5703/1288284316010

Huber, G., Haddock, J., Wielinski, J., Kriech, A., & Hekmatfar, A.. (2016, June 1–3). Adjusting design air void levels in Superpave mixtures to enhance durability. E&E Congress 2016, Prague, Czech Republic. https://www.h-a-d.hr/pubfile.php?id = 1091

Hughes, C. S. (1989). *Compaction of asphalt pavement* (National cooperative highway research program synthesis of highway practices No. 152).

Leiva, F., & West, R. C. (2008). Analysis of hot-mix asphalt lab compactability using lab compaction parameters and mix characteristics. *Transportation Research Record*, *2057*(1), 89–98. https://doi.org/10.3141/2057-11

Linden, R. N., Mahoney, J. P., & Jackson, N. C. (1989). Effect of compaction on asphalt concrete performance. *Transportation Research Record*, (1217), 20–28. https://trid.trb.org/view/306988

Liu, A. J., & Nagel, S. R. (1998). Jamming is not just cool any more. *Nature*, *396*(6706), 21–22. https://doi.org/10.1038/23819

Mamlouk, M. S., & Zaniewski, J. P. (2016). *Materials for Civil and construction engineers*, (4th ed., p. 197) Pearson Education, Incorporated.

Moutier, F. (1974). *La presse a cisaillement giratoire Modele*, de serie. Bull Liaison Lab, Ponts Chauss, (74).

Pine, W. J. (1997). *Superpave Gyratory compaction and the Ndesign table*. Illinois Department of Transportation.

Prowell, B. D., & Brown, E. R. (2007). *Superpave mix design: Verifying gyration levels in the Ndesign table* (Vol. 573). Transportation Research Board.

Prowell, B. D., Brown, E., & Huner, M. (2003). *Evaluation of the internal angle of gyration of superpave gyratory compactors in Alabama*. National Center for Asphalt Technology.

Sánchez-Leal, F. J. (2007). Gradation chart for asphalt mixes: Development. *Journal of Materials in Civil Engineering*, *19*(2), 185–197. https://doi.org/10.1061/(ASCE)0899-1561(2007)19:2(185)

Schofield, A. N., & Wroth, P. (1968). *Critical state soil mechanics* (Vol. 310). McGraw-Hill.

Shamsi, K., & Mohammad, L. N. (2010). Estimating optimum compaction level for dense-graded hot-mix asphalt mixtures. *The Journal of Engineering Research [TJER]*, *7*(1), 11–21. https://doi.org/10.24200/tjer.vol7iss1pp11-21

Stakston, A. D., & Bahia, H. U. (2003). *The effect of fine aggregate angularity, asphalt content and performance graded asphalts on hot mix asphalt performance* (Vol. 92, No. 45-98). Wisconsin Highway Research Program.

Vavrik, W. R., & Carpenter, S. H. (1998). Calculating air voids at specified number of gyrations in superpave gyratory compactor. *Transportation Research Record*, *1630*(1), 117–125. https://doi.org/10.3141/1630-14

Vavrik, W. R., Huber, G., Pine, W. J., & Carpenter, S. H. (2002). *Bailey method for gradation selection in hot-mix asphalt mixture design*. *Transportation research E-circular*, report No: E-C044.

Vivar, E. D. P., & Haddock, J. E. (2006). *HMA pavement performance and durability* (No. FHWA/IN/JTRP-2005/14).

Weisberg, S. (2014). *Applied linear regression*. John Wiley & Sons.

West, R., Rodezno, C., Leiva, F., & Yin, F. (2018). *Development of a framework for balanced mix design*. National Cooperative Highway Research (NCHRP) Project NCHRP, 20-07.

Yildirim, Y., Ideker, J., & Hazlett, D. (2006). Evaluation of viscosity values for mixing and compaction temperatures. *Journal of Materials in Civil Engineering*, *18*(4), 545–553. https://doi.org/10.1061/(ASCE)0899-1561(2006)18:4(545)